



Magnetic properties of synthesized cobalt–nickel ferrites ($\text{Co}_x\text{Ni}_{1-x}\text{Fe}_2\text{O}_4$) by hydrothermal method using malonic acid as a chelating agent

Saroj P. Sahare^{1,2} · Atul V. Wankhade² · Sangesh P. Zodape²

Received: 7 September 2022 / Accepted: 6 December 2022 / Published online: 17 December 2022
© The Author(s), under exclusive licence to Springer-Verlag GmbH, DE part of Springer Nature 2022

Abstract

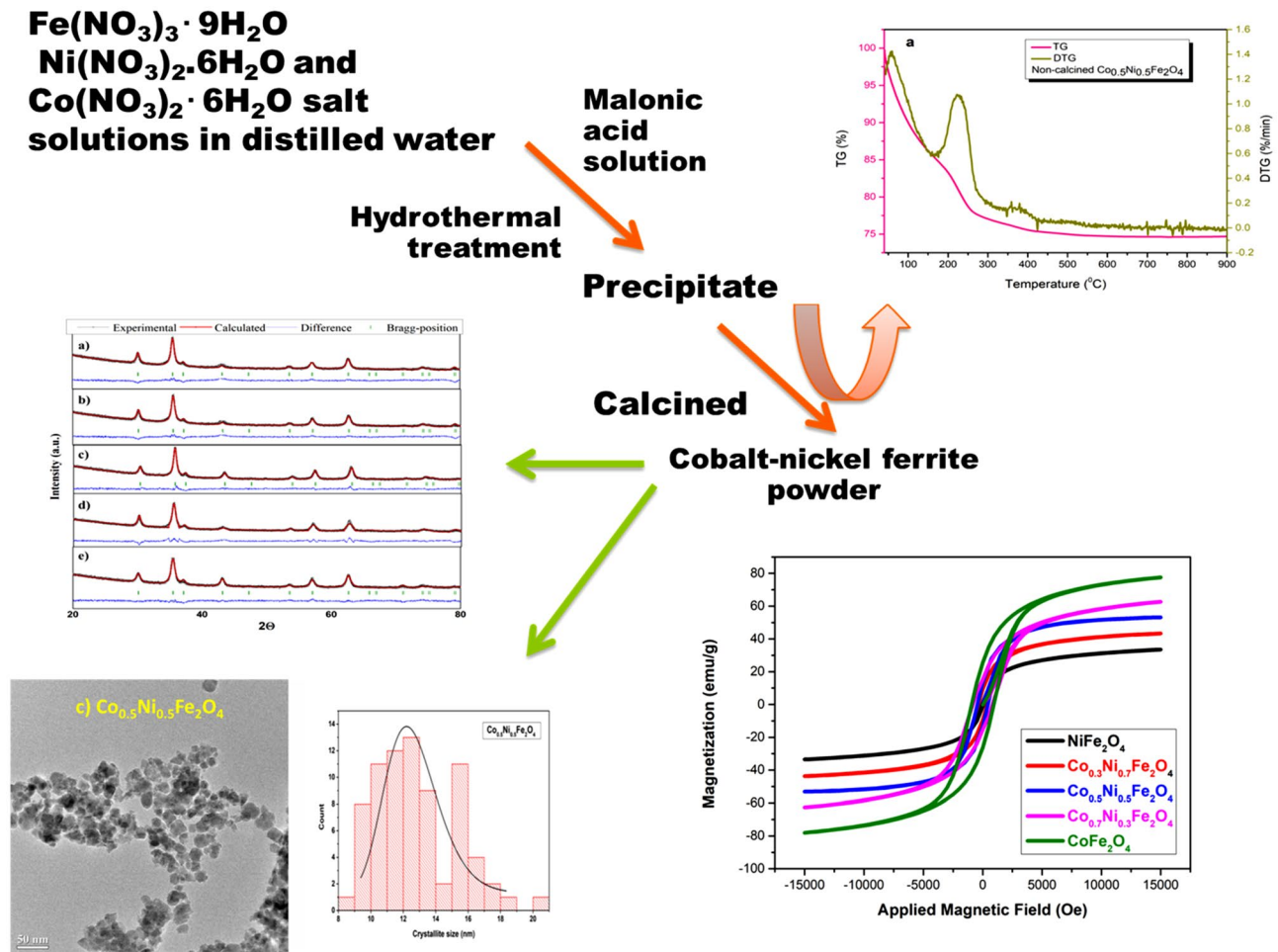
In the present study, cobalt–nickel ferrite nanoparticles ($\text{Co}_x\text{Ni}_{1-x}\text{Fe}_2\text{O}_4$ where $x = 0, 0.3, 0.5, 0.7,$ and 1) have been synthesized by the hydrothermal method assisted by malonic acid. Structural and morphological studies were accomplished by FTIR, XRD, XPS, FESEM, EDAX, and TEM. Structural and morphological studies illustrate single-phase spinel ferrites with monodispersed nanoparticles. Further, the average crystallite size was calculated by Debye–Scherrer’s equation. It was found between the ranges 7.9–15.4 nm for cobalt–nickel ferrites with varying cobalt mole fractions. Cobalt–nickel ferrite particles show a non-uniform particle shape which may be a result of its magnetic behavior (particle–particle attraction). Thermal gravimetric analysis was carried out to study the heat treatment process and to obtain the oxide phase. Also, magnetic properties were analyzed by taking the help of VSM. The saturation magnetization of nanoparticles remains within the range of 33.53–77.54 emu/g and coercivity lies between 50.50 and 933.69 Oe, respectively. In our study, a simple hydrothermal synthetic method assisted by malonic acid has been performed. It is quite environmentally friendly, economical and at the same time produces particles with small-size distribution. The synthesized cobalt–nickel ferrite samples are a promising candidate for high-density recording media.

✉ Sangesh P. Zodape
sangesh02@gmail.com

¹ Department of Chemistry, Anand Niketan College,
Warora 442 914, Maharashtra, India

² Department of Chemistry, Visvesvaraya National Institute
of Technology (VNIT), Nagpur 440 010, Maharashtra, India

Graphical abstract



Keywords Cobalt–nickel ferrite · Malonic acid · Hydrothermal synthesis · Magnetic property

1 Introduction

Recently, many scientific and research groups have been working on designing and enhancing the magnetic properties of ferrites [1–4]. Spinel ferrite has been a fascinating research topic in recent years because of its unique properties such as magnetic, optical, electrical, adsorption, sensor, and absorption [5–11]. As a result of their spectacular properties, the spinel ferrites find wide applicability in the fields of catalysis, photocatalytic, biomedical, environmental remediation, and memory devices [6, 12–15]. The molecular formula of inverse spinel ferrite is $\text{A}_x\text{B}_{1-x}\text{Fe}_2\text{O}_4$ (A, B = Co, Ni, Mg, etc.). It constitutes Fe^{3+} ions occupying both octahedral and tetrahedral interstitial sites and A^{2+} , and B^{2+} ions occupy octahedral interstitial sites [13]. Various synthesis techniques have been developed for ferrite nanoparticles, mostly hydrothermal synthesis, sol–gel

technique, solid-state reactions, co-precipitation, micro-emulsion, wet chemical process, and auto-combustion [16–24].

The exceptional magnetic properties of ferrite nanoparticles make them remarkable for many applications such as high-density recording media, microwave devices, and memory devices as well. Cobalt ferrite is generally known as a hard magnetic material that exhibits high coercivity and average magnetization while nickel ferrite is soft magnetic material [25, 26]. The effect of cobalt doping on nickel ferrites significantly affects the magnetic parameters which form the basis of understanding. The super-paramagnetic properties of ferrite nanoparticles are dependent on the shape, size, and purity of particles. These properties also depend on the initial parameters that have been selected during the process of synthesizing nanoparticles which are capable of altering the consequent nanostructure of the material [27, 28].

The particle size and saturation magnetization have been found to be improved for samples synthesized by the hydrothermal method over the sol–gel method [29]. The hydrothermal synthetic approach has been developed gradually into a most effective tool in material transformation in view of being environmentally favorable and extremely suitable for material processing, starting from bulk, fine, ultrafine, and finally nanoparticles. The hydrothermal technique aids the fabrication of composite materials along with motive physicochemical characteristics. It is the most preferred method over other conventional methods due to its simplicity, pollution-free, nucleation control, higher diffusion, and significantly accelerate rate of reaction and morphological control, respectively. The hydrothermal technique has ample benefits as it increases the interaction among solid and liquid species, transparency in the phase, and uniformity in the size of materials, and also, it improves the kinetics of the reaction. It is vital to note that, with the help of this method, the chemical atmosphere can be favorably tailored. Though there is a lightly prolonged reaction time, it yields appropriate crystalline controlled shape and size of nanoparticles [30].

The surface modification of spinel ferrites could be obtained through the use of a surfactant, chelating agent, capping agent, and organic moieties resulting in motive physicochemical characteristics [31]. There are different chelating agents used for the synthesis of cobalt and nickel ferrites including citric acid, sago starch, EDTA, oxalic acid, egg white, and tartaric acid. These reagents have some limitations such as polydisperse distribution of particles, a wider range of particle size, and mixed-phase of CoFe₂O₄ with α -Fe₂O₃ [32–34]. There are some investigations reported for carboxylic acid as a chelating agent along with fuel. Antic et al. reported the use of malonic acid in the synthesis of NiFe₂O₄, resulting in nanoparticles with a crystallite size of 11 nm. [35]. König et al. reported maleic acid as a chelating agent that gives pure phase spinel ferrite along with potential properties [36].

Considering these views, we are adopting a new protocol of synthesis for nanoparticles via the hydrothermal method by using malonic acid which acts as a chelating agent for the reduction in the particle size. Synthesized materials were characterized by FTIR, XRD, XPS, FESEM, EDAX, and TEM techniques. The outcomes of malonic acid as a chelating agent, in the process of approaching the structural, morphological, and magnetic properties of the cobalt–nickel ferrites, have been discussed in this work.

2 Experimental

2.1 Chemicals

Iron(III) nitrate nonahydrate (Fe(NO₃)₃·9H₂O, purity ≥ 98%, Alfa Aesar), cobalt(II) nitrate hexahydrate, (Co(NO₃)₂·6H₂O,

purity ≥ 98%, Alfa Aesar), nickel(II) nitrate hexahydrate (Ni(NO₃)₂·6H₂O, purity ≥ 98% Merck), malonic acid (CH₂(COOH)₂, purity ≥ 98%, Alfa Aesar), and potassium hydroxide (KOH, purity ≥ 84% Merck) were used. Chemicals were of analytical grade and used without further purification.

2.2 Synthesis of cobalt–nickel ferrites (Co_xNi_{1-x}Fe₂O₄ where x = 0, 0.3, 0.5, 0.7, and 1)

Cobalt–nickel ferrite nanoparticles were synthesized by using the hydrothermal method. For the synthesis of Co_{0.5}Ni_{0.5}Fe₂O₄, 0.2 M (50 mL) solution of iron (III) nitrate (Fe(NO₃)₃·9H₂O), 0.1 M (25 mL) solution of cobalt(II) nitrate (Co(NO₃)₂·6H₂O) and 0.1 M (25 mL) solution of nickel(II) nitrate (Ni(NO₃)₂·6H₂O) in distilled water were mixed with an aqueous solution of malonic acid under vigorous stirring. The molar ratio of malonic acid and metal ions was kept at 3:1 for the complete chelation of metal ions. Malonic acid is used as a chelating agent for metal ions in this process. To maintain alkaline pH (~11), aqueous solution of KOH (2 M) was added. The reaction mixture was transferred into a Teflon-lined stainless steel autoclave (400 mL capacity) and kept in an oven for 12 h at 100 °C. The obtained precipitate was washed with distilled water until pH became neutral and dried in an oven, and used further for thermogravimetric and infrared spectroscopic analysis.

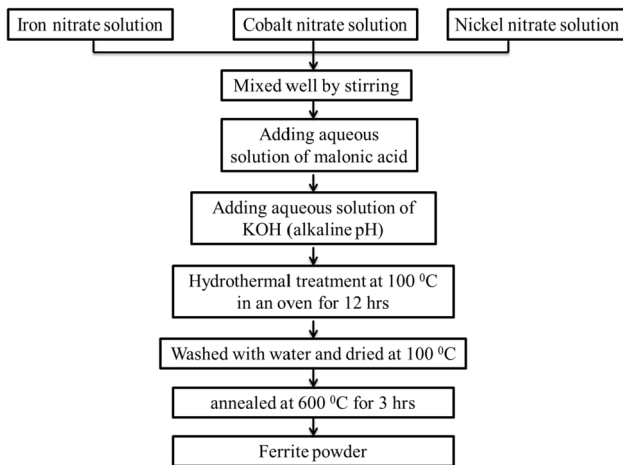
The above procedure was repeated for the synthesis of cobalt ferrite (CoFe₂O₄), nickel ferrite (NiFe₂O₄), and cobalt–nickel ferrites (Co_xNi_{1-x}Fe₂O₄ where x = 0.3 and 0.7) with different molar ratios of metal ions as shown in Table 1. All the samples have been annealed at 600 °C for 3 h, crushed into a fine powder, and used for further analysis. A chart for synthesis of cobalt–nickel ferrites is shown in Fig. 1.

2.3 Characterization

The material structure and phase purity were determined with an X-ray diffractometer (Bruker AXS D8 Advance) with monochromatic Cu K_α radiation (40 kV, 35 mA). The values of wavelength and 2θ are 1.5406 Å and 20°–80°, respectively. The morphology of the material was investigated by field emission scanning electron microscope (FESEM) by using an instrument (JEOL 6380A) with energy-dispersive X-ray spectroscopy by Joel (JSM 5400) apparatus and transmission electron microscopy (TEM) using a JSM-100CX, Joel instrument. The thermogravimetric analysis was done using a TG-DTA-7200 (Hitachi) Universal Testing Machine H10KT (Tinius Olsen) instrument. X-ray photoelectron spectroscopy (XPS) was studied at Beamline (BL-14) RRCAT, Indore. Infrared spectroscopy

Table 1 Experimental conditions employed to synthesize the $\text{Co}_x\text{Ni}_{1-x}\text{Fe}_2\text{O}_4$ nanoparticles (where $x=0, 0.3, 0.5, 0.7, \text{ and } 1$)

Sr. No.	Composition	Iron (III) nitrate (0.2 M) (mL)	Nickel (II) nitrate (0.1 M) (mL)	Cobalt (II) nitrate (0.1 M) (mL)
1.	NiFe_2O_4	50	50	–
2.	$\text{Co}_{0.3}\text{Ni}_{0.7}\text{Fe}_2\text{O}_4$	50	35	15
3.	$\text{Co}_{0.5}\text{Ni}_{0.5}\text{Fe}_2\text{O}_4$	50	25	25
4.	$\text{Co}_{0.7}\text{Ni}_{0.3}\text{Fe}_2\text{O}_4$	50	15	35
5.	CoFe_2O_4	50	–	50

**Fig. 1** A chart of synthesis method of cobalt–nickel ferrites

studies were carried out by operating infrared spectrometers (Shimadzu-IR Affinity-1). The magnetic properties of synthesized samples were studied by using Vibrating Sample Magnetometer (Lakeshore, USA, Model 7407).

3 Results and discussion

3.1 Powder X-ray diffraction studies

Figure 2 represents the XRD patterns of synthesized calcined cobalt–nickel ferrite, cobalt ferrite, and nickel ferrite nanoparticles. The characterization peaks in the diffraction pattern observed at 2θ values 30.3, 35.7, 37.3, 43.3, 53.6, 57.4, 62.6, and 30.2, 35.6, 37.3, 43.2, 53.6, 57.4, 62.7 corresponded to the miller indices (220), (311), (222), (400), (422), (511), (440) for nickel ferrite and cobalt ferrite, respectively, were matched with the standard JCPDS files 10-0325 (nickel ferrite) and 22-1086 (cobalt ferrite) [37]. This confirms the successful synthesis of cobalt ferrite and nickel ferrite. In the case of cobalt–nickel ferrites, the 2θ values and corresponding miller indices were matched with reported values in both the JCPDS files of cobalt ferrite and nickel ferrite. This provides clear evidence

of cobalt–nickel ferrites ($\text{Co}_{0.3}\text{Ni}_{0.7}\text{Fe}_2\text{O}_4$, $\text{Co}_{0.5}\text{Ni}_{0.5}\text{Fe}_2\text{O}_4$, and $\text{Co}_{0.7}\text{Ni}_{0.3}\text{Fe}_2\text{O}_4$) formation and the diffraction pattern indicates fabrication of a cubic spinel structure. It is noticed from FTIR studies (shown in Fig. 7) that malonic acid acts as a chelating agent and forms metal malonate complexes from metal nitrates. These outcomes contribute to the slow migration of bulkier metal malonates as compared to the fast migration of lighter cobalt/nickel/ferric ions (without a chelating agent) during the calcination process. The slow migration of cobalt/nickel/ferric malonates allows plenty of time to occupy an accurate location in the crystal lattice leading to more peaks (vide infra) [38].

The lattice constant increases with cobalt content due to a greater ionic radius of Co^{2+} (0.78 Å) compared to Ni^{2+} (0.74 Å) as expected from the literature [39]. The average crystallite size (D_{XRD}) of cobalt–nickel ferrites is (shown in Table 2) calculated from the Debye–Scherrer's equation [$D = 0.9\lambda/\beta \cos \theta$], where the λ is the wavelength of X-ray radiation (1.5406 Å), β is full-width half maxima (FWHM), where θ is for Bragg's angle of X-ray diffraction peak. The cell parameters were calculated from XRD spectra by Rietveld refinement [40, 41]. The XRD patterns of cobalt–nickel ferrites (synthesized without malonic acid) are shown in Fig. S1 and parameters are depicted in Table S1 in supporting information. The X-ray diffraction patterns of two samples ($\text{Co}_x\text{Ni}_{1-x}\text{Fe}_2\text{O}_4$, where $x=0.3$ and 0.7) before thermal treatment were shown in Fig. S2 (supporting information) to analyze the crystalline nature of samples. It is observed that samples are not in spinel crystalline form. The spinel ferrite structures are formed after the thermal treatment of samples. The same results are observed from the thermogravimetric studies, where the calcined sample does not show significant weight loss but non-calcined samples (before heat treatment) show weight losses due to malonic acid chelation complex.

3.2 Morphological studies

3.2.1 Field emission scanning electron microscopic (FESEM) studies

The FESEM images of cobalt–nickel ferrites ($\text{Co}_{0.5}\text{Ni}_{0.5}\text{Fe}_2\text{O}_4$ and $\text{Co}_{0.7}\text{Ni}_{0.3}\text{Fe}_2\text{O}_4$) before and after

Fig. 2 XRD patterns of cobalt–nickel ferrites: **a** NiFe₂O₄, **b** Co_{0.3}Ni_{0.7}Fe₂O₄, **c** Co_{0.5}Ni_{0.5}Fe₂O₄, **d** Co_{0.7}Ni_{0.3}Fe₂O₄, and **e** CoFe₂O₄ nanoparticles

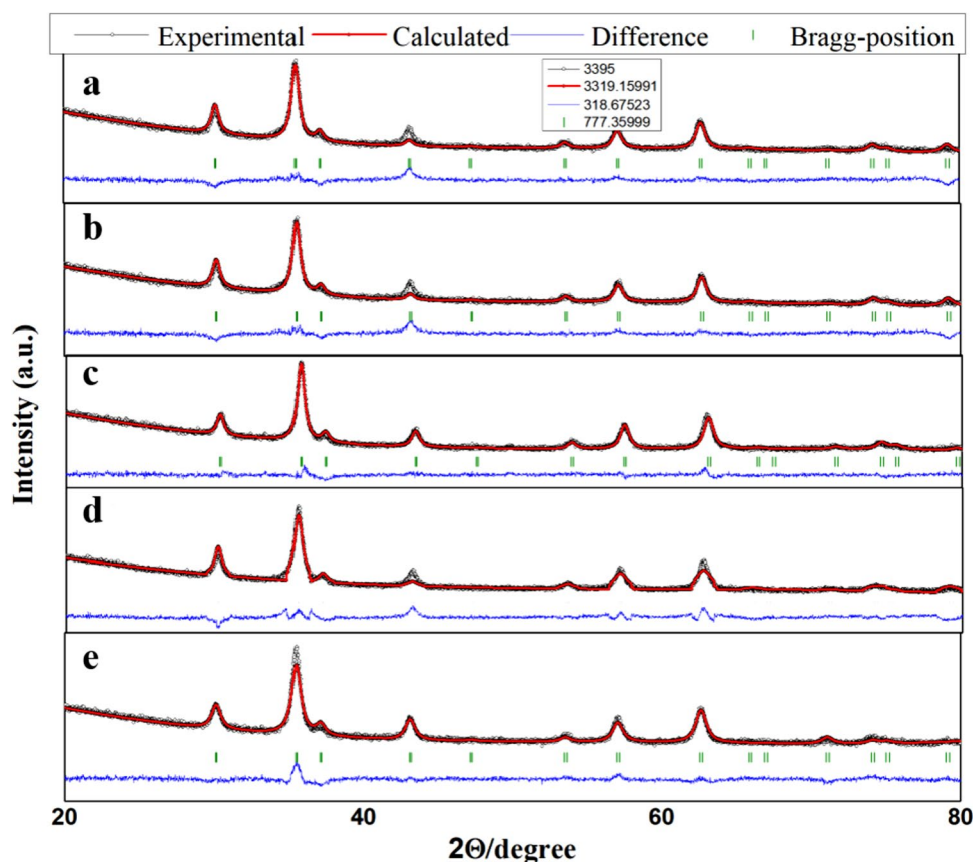


Table 2 Cobalt–nickel mixed ferrites (Co_xNi_{1-x}Fe₂O₄) composition with D_{XRD} , lattice parameter, and volume

Composition	D_{XRD} (nm)	Lattice parameter (Å)	Volume (Å ³)	χ^2 (chi ²)
NiFe ₂ O ₄	7.90	8.331	578.22	1.57
Co _{0.3} Ni _{0.7} Fe ₂ O ₄	9.52	8.336	579.26	1.23
Co _{0.5} Ni _{0.5} Fe ₂ O ₄	10.16	8.340	580.10	1.19
Co _{0.7} Ni _{0.3} Fe ₂ O ₄	12.42	8.344	580.93	1.34
CoFe ₂ O ₄	15.43	8.353	582.81	1.12

calcination are shown in Fig. 3 at different magnifications. Figure 3a, b, e, and f images of non-calcined (Co_{0.5}Ni_{0.5}Fe₂O₄ and Co_{0.7}Ni_{0.3}Fe₂O₄) samples reveal that there is no certain border between particles, and they are agglomerated. The particles are not in cubic spinel ferrite form as observed from the XRD patterns of non-calcined samples and from the IR spectrum which indicates a complex stage of metal ions with malonic acid for non-calcined samples. During the calcination process, the particles rearranged and became spherical as observed in Fig. 3c, d, g, and h of calcined samples [29]. During the heat treatment process, particles are developed into spinel ferrites as observed from thermogravimetric studies (that non-calcined samples

are converted into oxide form after 550 °C). After heat treatment, the particles converted into spinel form as observed from XRD patterns of calcined samples. Therefore, calcined samples (Fig. 3d and h) shows certain boundaries between particles with spherical shape.

3.2.2 Energy-dispersive X-ray spectroscopic (EDAX) studies

The EDAX spectrums of cobalt–nickel ferrite (Co_{0.5}Ni_{0.5}Fe₂O₄ and Co_{0.7}Ni_{0.3}Fe₂O₄) samples (Fig. 4a and c non-calcined and b and d calcined) are shown in Fig. 4. The spectrums of non-calcined cobalt–nickel ferrites [Fig. 4a (Co_{0.5}Ni_{0.5}Fe₂O₄) and c (Co_{0.7}Ni_{0.3}Fe₂O₄)] indicates the presence of carbon peak along with the constituent elements (cobalt, nickel, iron, and oxygen). The presence of carbon is predicted due to the complex formation of metal ions with malonic acid. The same is observed from the IR spectrum of non-calcined samples. The non-calcined samples are in the complex stage and not in the ferrite form. This is also observed in TGA and XRD studies. The spectrums of calcined cobalt–nickel ferrites (Fig. 4b) Co_{0.5}Ni_{0.5}Fe₂O₄ and d (Co_{0.7}Ni_{0.3}Fe₂O₄) exhibit peaks of constituent elements (cobalt, nickel, iron, and oxygen). The above studies revealed the presence of Co, Ni, Fe, and O in the synthesized cobalt–nickel ferrite. After calcination, the samples

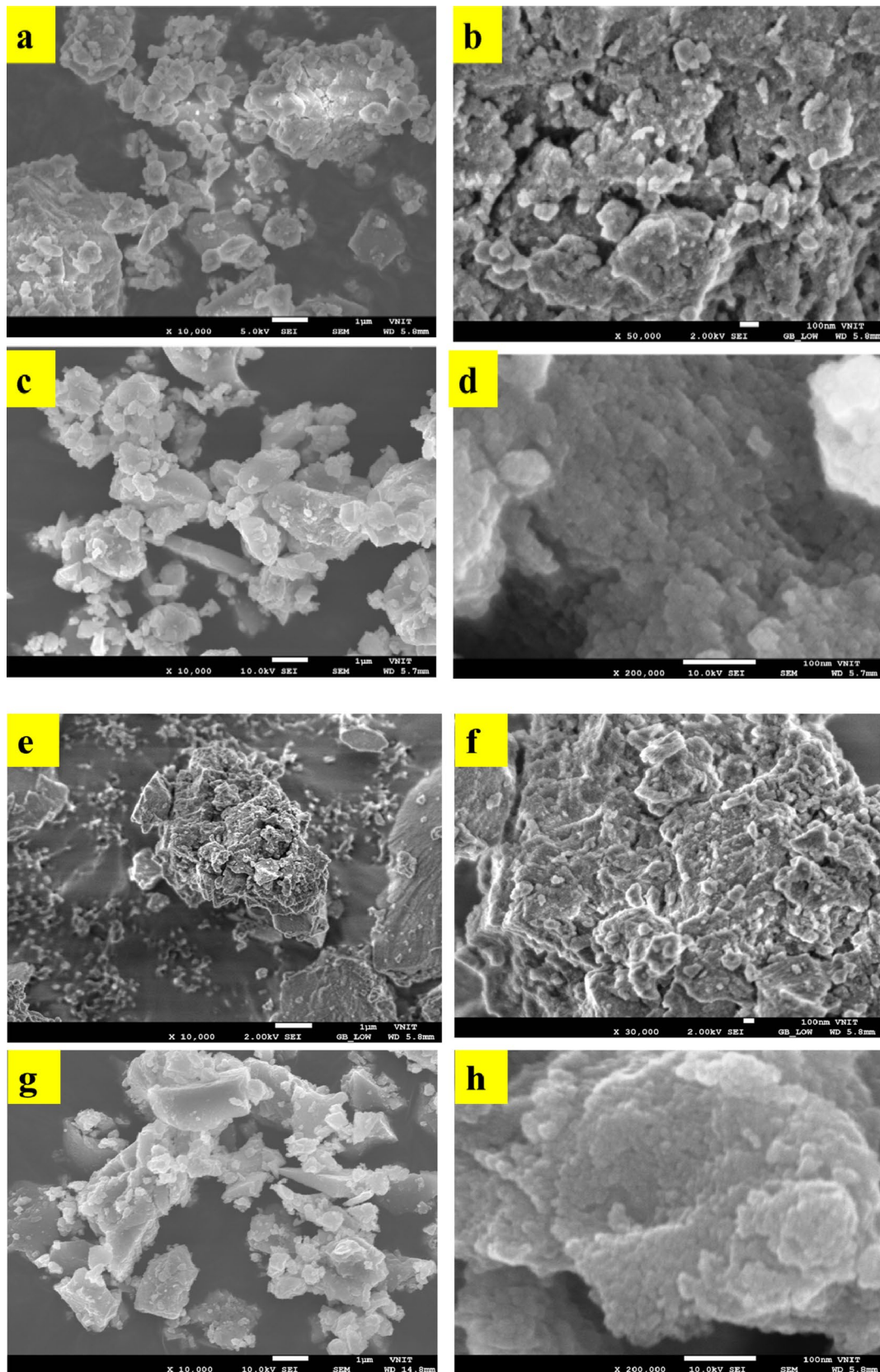


Fig. 3 FESEM micrographs of cobalt–nickel ferrite at different magnifications: **a** ($\text{Co}_{0.5}\text{Ni}_{0.5}\text{Fe}_2\text{O}_4$) non-calcined-1 μ , **b** ($\text{Co}_{0.5}\text{Ni}_{0.5}\text{Fe}_2\text{O}_4$) non-calcined-100 nm, **c** ($\text{Co}_{0.5}\text{Ni}_{0.5}\text{Fe}_2\text{O}_4$) calcined-1 μ , **d**

($\text{Co}_{0.5}\text{Ni}_{0.5}\text{Fe}_2\text{O}_4$) calcined-100 nm, **e** ($\text{Co}_{0.7}\text{Ni}_{0.3}\text{Fe}_2\text{O}_4$) non-calcined-1 μ , **f** ($\text{Co}_{0.7}\text{Ni}_{0.3}\text{Fe}_2\text{O}_4$) non-calcined-100 nm, **g** ($\text{Co}_{0.7}\text{Ni}_{0.3}\text{Fe}_2\text{O}_4$) calcined-1 μ , **h** ($\text{Co}_{0.7}\text{Ni}_{0.3}\text{Fe}_2\text{O}_4$) calcined-100 nm

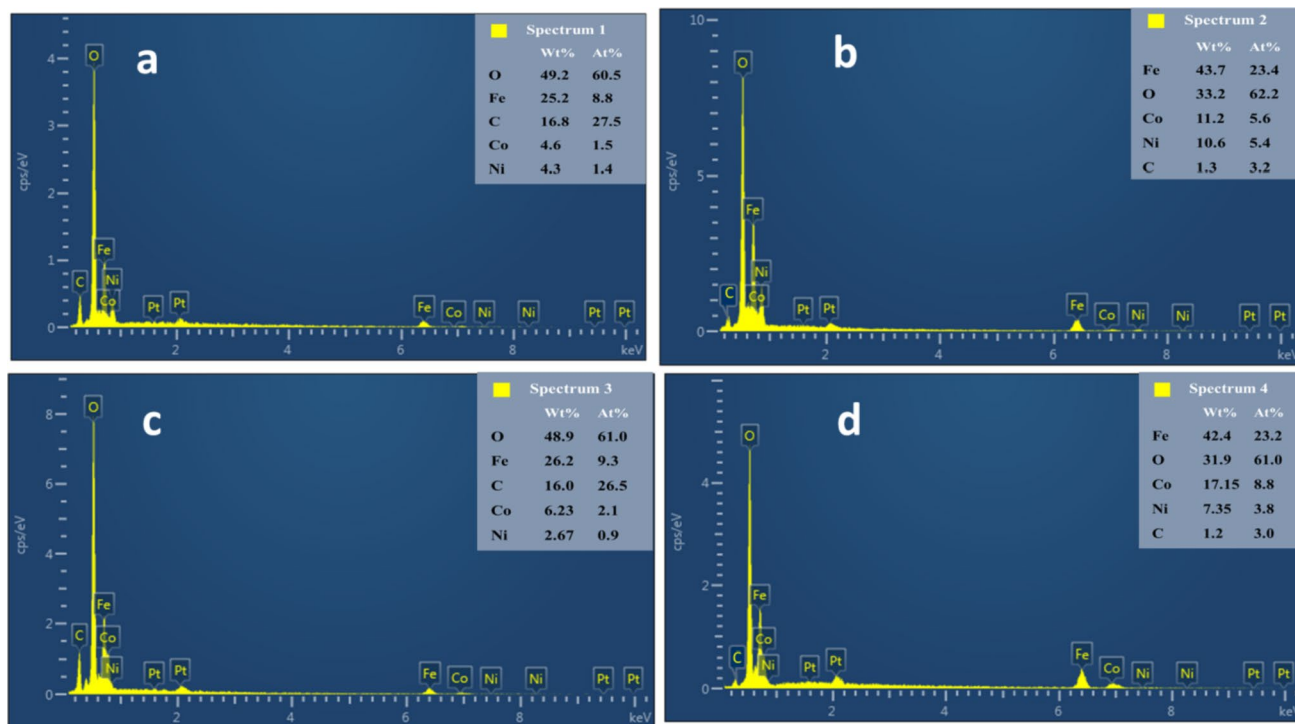


Fig. 4 EDAX spectra of cobalt–nickel ferrites: **a** ($\text{Co}_{0.5}\text{Ni}_{0.5}\text{Fe}_2\text{O}_4$) non-calcined, **b** ($\text{Co}_{0.5}\text{Ni}_{0.5}\text{Fe}_2\text{O}_4$) calcined, **c** ($\text{Co}_{0.7}\text{Ni}_{0.3}\text{Fe}_2\text{O}_4$) non-calcined, and **d** ($\text{Co}_{0.7}\text{Ni}_{0.3}\text{Fe}_2\text{O}_4$) calcined

are converted into spinel ferrites as observed from XRD patterns, and hence, the weak carbon peak that appeared in calcined cobalt–nickel ferrite may be due to carbon tape which is used during FESEM and EDS experiments.

3.2.3 Transmission electron microscopic (TEM) studies

The TEM micrographs of cobalt-substituted nickel ferrites ($\text{Co}_x\text{Ni}_{1-x}\text{Fe}_2\text{O}_4$, where $x=0, 0.3, 0.5, 0.7$, and 1) are shown in Fig. 5, the TEM images and corresponding histograms revealed the particle size of ferrite samples. Nickel ferrite particles have a size distribution in the range of 6–16 nm with an average particle size of 10 nm shown in Fig. 5a. In Fig. 5b, $\text{Co}_{0.3}\text{Ni}_{0.7}\text{Fe}_2\text{O}_4$ ferrite shows particles distribution in the range of 6–22 nm and an average particle size of 12 nm. Cobalt–nickel mixed ferrites of composition $\text{Co}_{0.5}\text{Ni}_{0.5}\text{Fe}_2\text{O}_4$ show particle distribution of 8–20 nm in Fig. 5c with an average dopant size of 13 nm. In Fig. 5d, $\text{Co}_{0.7}\text{Ni}_{0.3}\text{Fe}_2\text{O}_4$ ferrite particles show the particles in the range of 10–24 nm, and the average particle size was found to be 17 nm. These results are in agreement with XRD data. Cobalt ferrite particles are in the range of 8–24 nm and the average dopant size is 17 nm as shown in Fig. 5e. The TEM images indicate that the particles are not regular in shape. Non-uniformity in shape is due to particle agglomeration and the magnetic behavior of particles (particle–particle attraction) [29].

3.3 X-ray photoelectron spectroscopic (XPS) studies

To obtain the surface composition with the chemical state of cobalt, nickel, and iron on the surface of cobalt–nickel ferrite ($\text{Co}_{0.5}\text{Ni}_{0.5}\text{Fe}_2\text{O}_4$), the sample was examined by XPS and wide-scan spectra in the binding energy range of 200–1000 eV as depicted in Fig. 6. The XPS spectra of cobalt–nickel ferrite indicates the presence of Co, Ni, Fe, and O atoms. In $\text{Co}_{0.5}\text{Ni}_{0.5}\text{Fe}_2\text{O}_4$ ferrite, iron ions are in a +3 oxidation state. The photoelectronic peak for $\text{Fe}2p_{3/2}$ (Fig. 6b) is split into two subpeaks upon fitting at 709.11 and 712.4 eV (main peaks, Fe^{3+}) and a satellite peak observed at 716.2 eV. The $\text{Fe}2p_{1/2}$ fitting peak at 724.3 eV was marked to Fe^{3+} and the results are in good agreement with previously studied iron oxide compounds [42–44]. The $\text{Co}2p_{3/2}$ photoelectronic peaks depicted in Fig. 6c suggest the presence of Co^{2+} . The spectrum shows two spin-orbital doublets $\text{Co}2p_{3/2}$ (778.4 eV, B sites and 780.6 eV, A sites) with a corresponding satellite peak at 784.9 eV [43, 45, 46]. The photoelectronic peak for $\text{Ni}2p_{3/2}$ (Fig. 6d) is observed at 854.4 eV, which is in accordance with the previously studied nickel ferrite [39]. The peaks for O1 and O2 (Fig. 6e) are observed at 529.8 and 531.2 eV, respectively. The peak O1 (529.8 eV) represented a metal–oxygen bond and peak O2 (531.2 eV) corresponded to O in a multiplicity of chemisorbed water at the surface [43, 44]. XPS studies reveal that $\text{Co}_{0.5}\text{Ni}_{0.5}\text{Fe}_2\text{O}_4$ ferrite has been synthesized successfully.

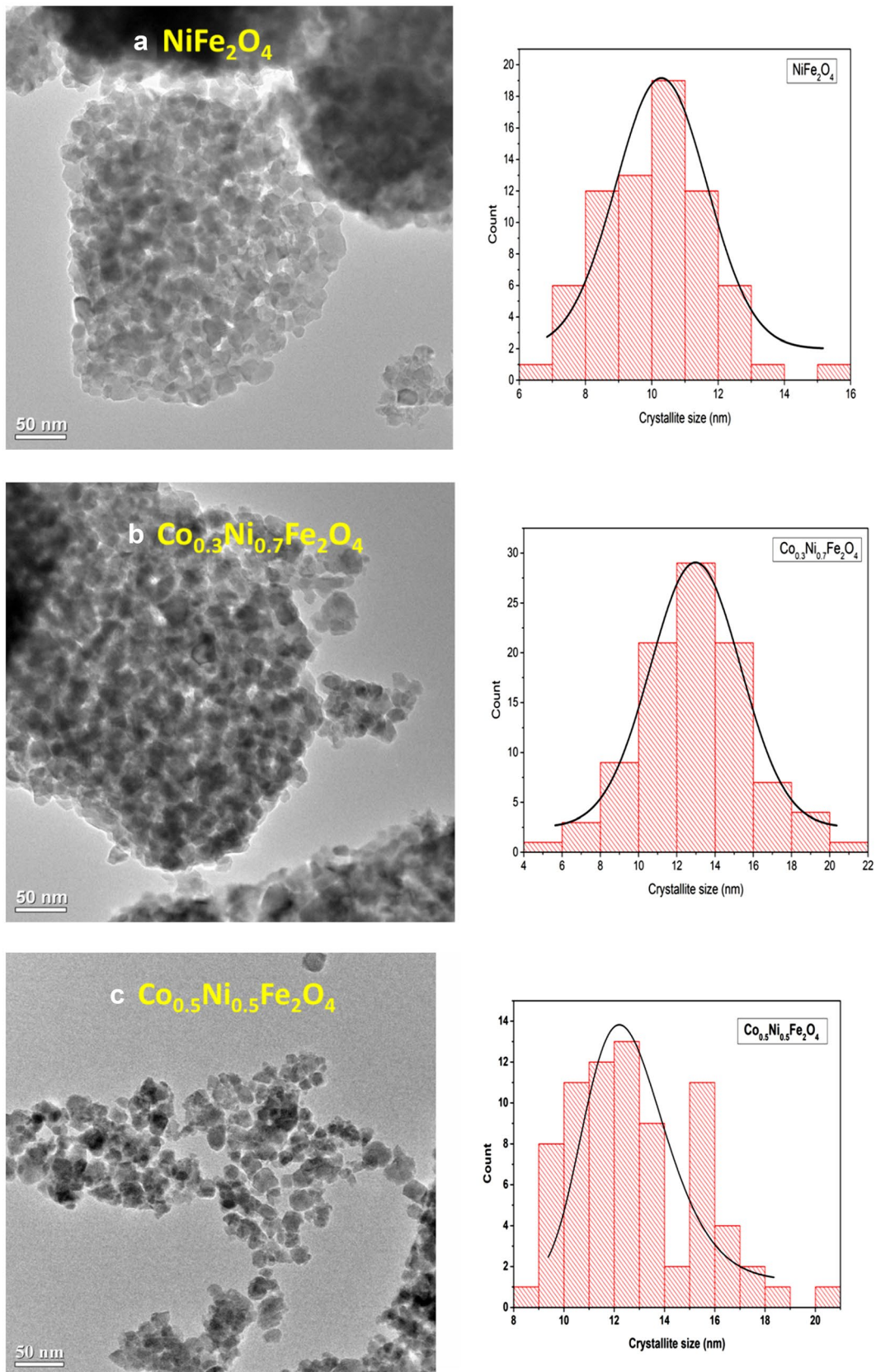


Fig. 5 TEM images and their corresponding histograms of **a** NiFe_2O_4 , **b** $\text{Co}_{0.3}\text{Ni}_{0.7}\text{Fe}_2\text{O}_4$, **c** $\text{Co}_{0.5}\text{Ni}_{0.5}\text{Fe}_2\text{O}_4$, **d** $\text{Co}_{0.7}\text{Ni}_{0.3}\text{Fe}_2\text{O}_4$, and **e** CoFe_2O_4 ferrites

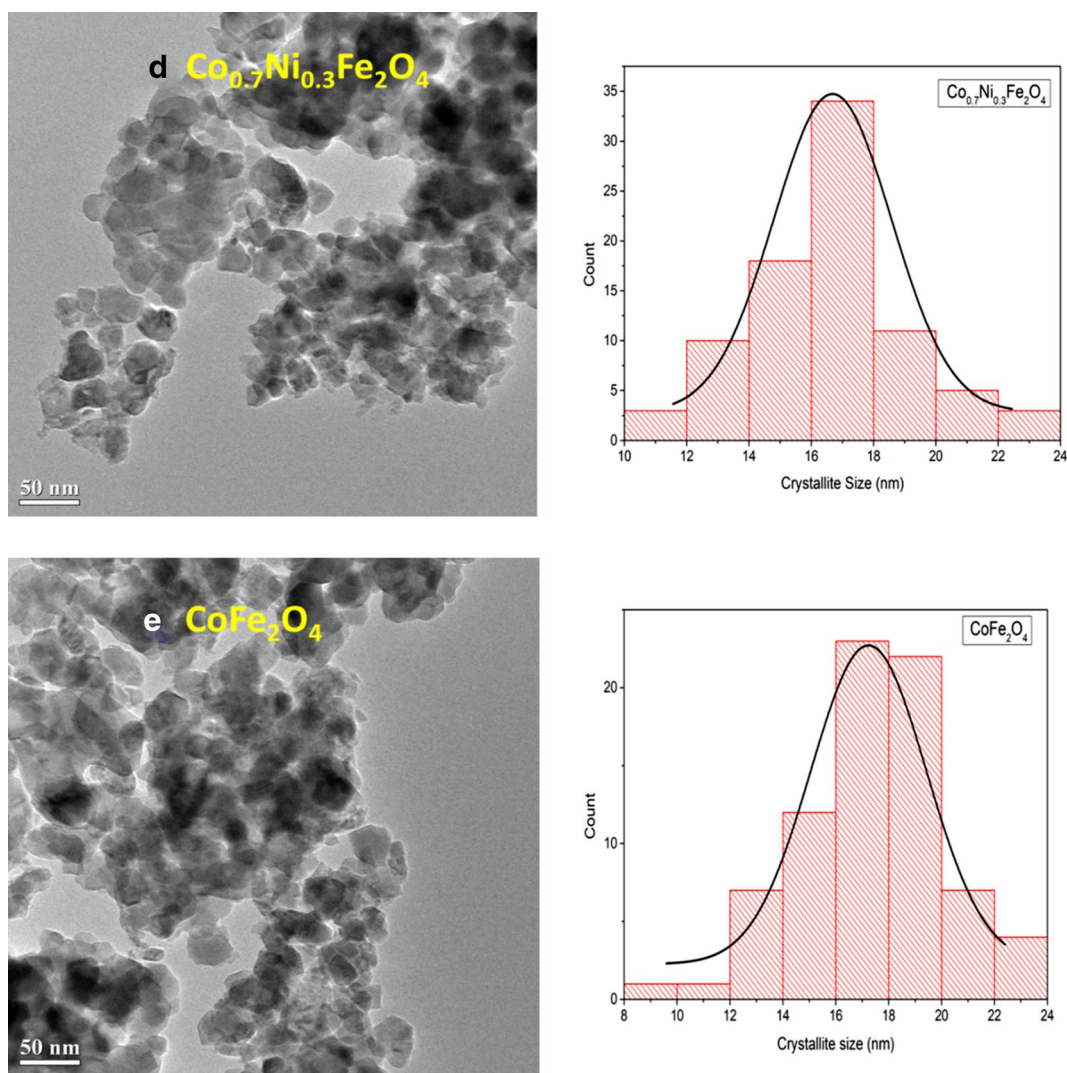


Fig. 5 (continued)

3.4 Fourier transform infrared spectroscopic studies

The FTIR spectra of non-calcined and calcined samples of ferrite are shown in Fig. 7a and b. The spectrum corresponding to non-calcined cobalt–nickel ferrites (CoFe_2O_4 , NiFe_2O_4 , $\text{Co}_{0.5}\text{Ni}_{0.5}\text{Fe}_2\text{O}_4$) shows a peak around 3195, 3200, and 3110 cm^{-1} attributed to stretching vibrations of hydroxyl groups. The weak peaks were observed at 2854, 2929, and 2921 cm^{-1} due to aliphatic C–H stretching in CoFe_2O_4 , NiFe_2O_4 , and $\text{Co}_{0.5}\text{Ni}_{0.5}\text{Fe}_2\text{O}_4$, respectively. The two bands were observed at 1588 and 1384 cm^{-1} for asymmetric $\nu_{\text{as}}(\text{COO})$ and symmetric $\nu_{\text{s}}(\text{COO})$ stretching vibrations of COO groups, respectively, in $\text{Co}_{0.5}\text{Ni}_{0.5}\text{Fe}_2\text{O}_4$. Also, these bands are observed at 1571 and 1339 cm^{-1} in CoFe_2O_4 and 1571 and 1320 cm^{-1} in NiFe_2O_4 . These bands confirm the coordination of metal ions by

carboxylate groups to form a chelate complex [38, 47]. The bands observed in the range 400–600 cm^{-1} are a result of M–O stretching. Figure 7b shows the FTIR spectrum of calcined samples of cobalt ferrite (CoFe_2O_4), nickel ferrite (NiFe_2O_4), and cobalt–nickel ferrite ($\text{Co}_{0.5}\text{Ni}_{0.5}\text{Fe}_2\text{O}_4$). The two bands were observed in the region of 400–600 cm^{-1} for all spinel ferrites [48]. The bands at 589 and 418 cm^{-1} are due to tetrahedral and octahedral vibrational stretching in cobalt ferrite. The bands at 592 and 415 cm^{-1} are observed for M–O vibrational stretching which are characteristic peaks of nickel ferrite. The vibrating bands at 556 and 444 cm^{-1} are observed for metal oxide (M–O) vibrational stretching in cobalt–nickel ferrite ($\text{Co}_{0.5}\text{Ni}_{0.5}\text{Fe}_2\text{O}_4$), characteristic of spinel ferrite. The absence of organic bands indicates the decomposition of organic moieties after calcination and organic-free cobalt–nickel ferrite formation occurred.

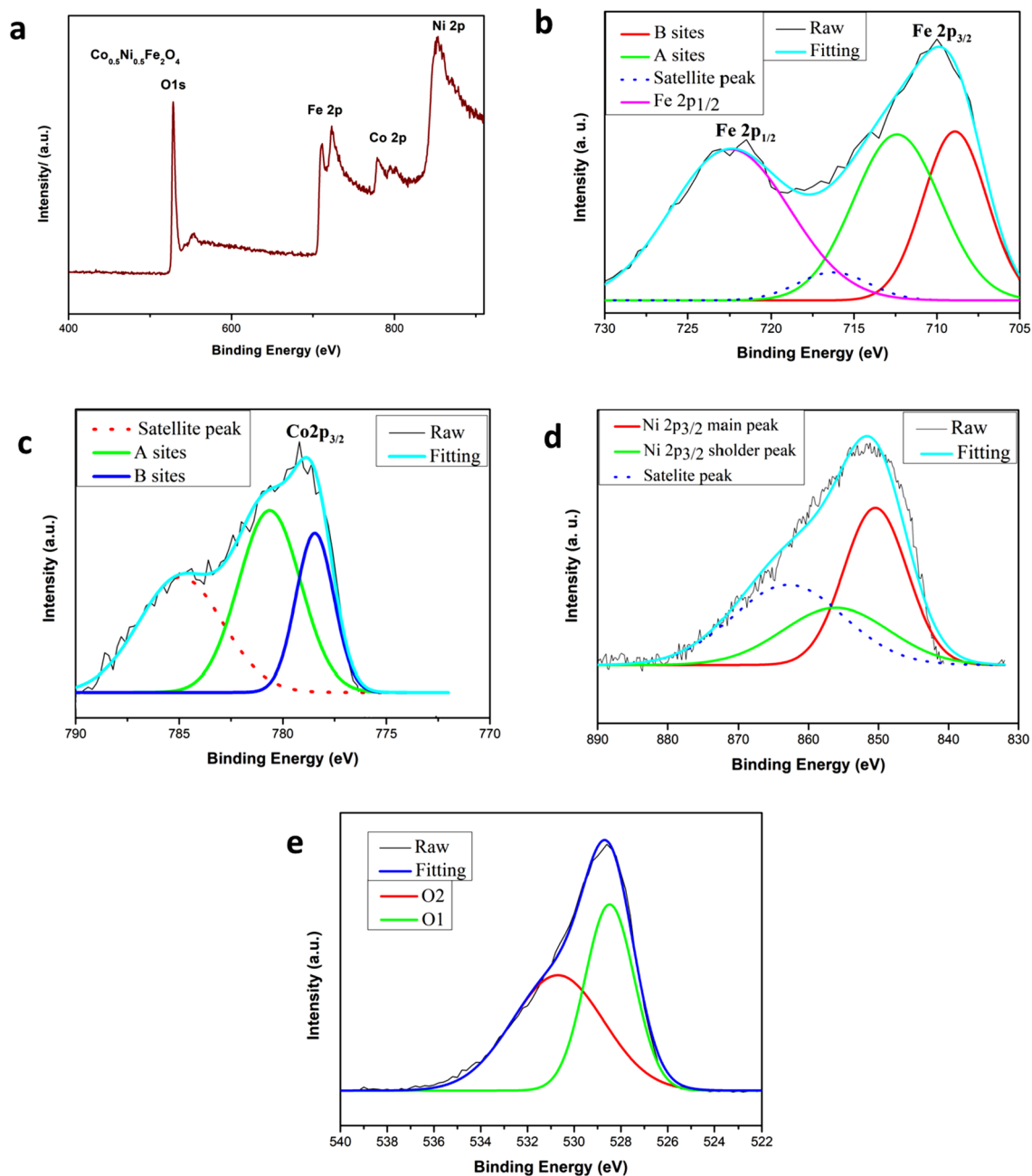


Fig. 6 XPS spectra of cobalt–nickel ferrite ($\text{Co}_{0.5}\text{Ni}_{0.5}\text{Fe}_2\text{O}_4$): **a** survey spectrum, **b** Fe 2p spectrum, **c** Co 2p spectrum, **d** Ni 2p spectrum, and **e** O1s spectrum

3.5 Thermal gravimetric studies

The TG/DTG curves of non-calcined and calcined cobalt–nickel ferrites are shown in Fig. 8a (NiFe_2O_4), b (CoFe_2O_4), c ($\text{Co}_{0.5}\text{Ni}_{0.5}\text{Fe}_2\text{O}_4$), and d ($\text{Co}_{0.5}\text{Ni}_{0.5}\text{Fe}_2\text{O}_4$). The thermogravimetric analysis was carried out from 40 to 900 °C. Figure 8a corresponds to the non-calcined nickel ferrite. The weight loss is observed up to 450 °C in three steps. In the first step, weight loss is observed due to absorbed

water up to 140 °C. The next weight loss is observed up to 300 °C because of organic matter decomposition. Further weight loss (up to 410 °C) is observed due to the oxidation of metal ions and the formation of spinel ferrite. Figure 8b of CoFe_2O_4 shows weight loss up to 400 °C. The first weight loss (up to 190 °C) indicates loss of moisture, and the next weight loss (up to 310 °C) is because of organic matter decay. Further loss (up to 400 °C) indicates oxidation of metal ions and formation of ferrites. The curve shown in

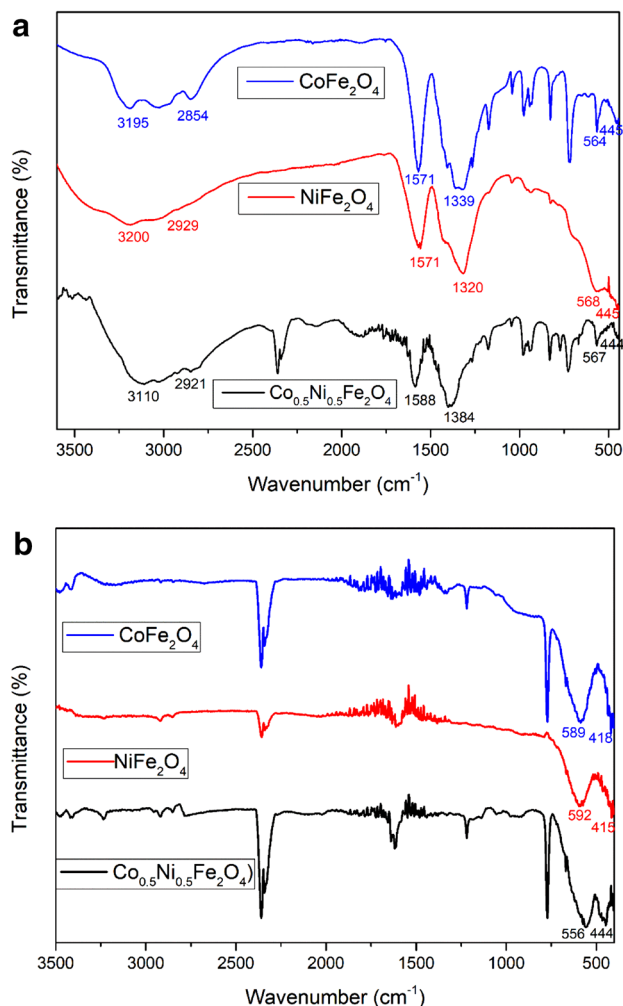


Fig. 7 FTIR spectra of **a** non-calcined cobalt ferrite (CoFe₂O₄), nickel ferrite (NiFe₂O₄), and cobalt nickel ferrite (Co_{0.5}Ni_{0.5}Fe₂O₄), **b** calcined samples of cobalt ferrite (CoFe₂O₄), nickel ferrite (NiFe₂O₄), and cobalt nickel ferrite (Co_{0.5}Ni_{0.5}Fe₂O₄)

Fig. 8c corresponds to non-calcined cobalt–nickel ferrite. It is observed that weight loss is up to 550 °C by three decomposition steps. The first weight loss occurred between 40 and 160 °C in the TG curve having a peak at 60 °C in the DTG curve due to the loss of water molecules. Immediately the weight loss observed up to 300 °C in the TG curve and the peak at 230 °C in the DTG curve contribute to the decomposition of organic matter. Further slow weight loss is observed up to 550 °C indicating oxidation of organic matter. No significant weight loss is observed above 550 °C. This provides information about the heat treatment process [49, 50]. The thermogravimetric analysis for calcined cobalt–nickel ferrite is shown in Fig. 8d. The TG/DTG analysis was performed in the range of 40–900 °C. The weight loss is negligible for calcined cobalt–nickel ferrite indicating an oxide phase. The same is observed from XRD patterns of calcined samples,

which show the ferrite phase while the non-calcined samples do not show the spinel ferrite phase. Also, IR spectrum of non-calcined samples revealed the presence of organic compounds (malonic acid chelation) while calcined did not. The results are in agreement with FTIR and XRD studies. The TG curve for the sample synthesized without malonic acid chelation is shown in Fig. S3 in the supporting information. The curve shows concurrent weight loss up to 400 °C indicating the conversion of metal ions from hydroxide to oxide phase.

3.6 Magnetic properties

The room temperature magnetization curves of Co_xNi_{1-x}Fe₂O₄ nanoparticles are depicted in Fig. 9. The values of coercivity (H_c), saturation magnetization (M_s), remanent magnetization (M_r), and squareness parameter (M_r/M_s) with different compositions of Co_xNi_{1-x}Fe₂O₄ nanoparticles evaluated from hysteresis loops are tabulated in Table 3. The saturation magnetization is determined significantly less than the bulk counterpart with 50 emu/g for nickel ferrite and up to 88 emu/g for cobalt ferrite [49, 50]. The s-shape of the M–H curve at the lower field increases linearly at a higher field indicating the presence of small magnetic particles exhibiting super-paramagnetic behaviors [37, 51]. Super-paramagnetism is the non-retainment of any magnetism after the removal of the applied magnetic field is a principally necessary property for magnetic target carriers [52]. The super-paramagnetism is a type of magnetism that emerges in small-size ferromagnetic or ferrimagnetic nanoparticles [53]. Our results show the smaller size (7.9–15.4 nm) from XRD studies. The magnitudes of M_s achieved by us are 33.53 and 77.54 emu/g for NiFe₂O₄ and CoFe₂O₄, respectively. Our values for M_s are comparable with the observation of Kamellia et al. (34.45 emu/g) and Young et al. (78.0 emu/g) [54, 55]. In addition to these, the obtained values are slightly higher than those examined by Kolekar et al. (28 emu/g) and Shah et al. (65 emu/g) [56, 57].

The magnetization of nickel ferrite depends upon the exchange interaction between tetrahedral and octahedral sublattices. The magnetic property of NiFe₂O₄ is the cumulative effect of magnetocrystalline anisotropy, dipole interactions on the surface of nanoparticles, and canting effect interactions [58]. The small coercivity observed from the hysteresis curve revealed that the coalescence of the crystallites increased in the nanostructure which enhanced magnetic coupling and higher magnetization. The magnitude of saturation magnetization, remanent magnetization, and coercivity are highly affected by cobalt doping. The coercivity (H_c) increases with enhanced cobalt contents due to the greater anisotropic nature of cobalt than nickel. The enhancement in coercivity with cobalt doping observed from the M–H curve is associated with improvement in the anisotropic field, which in turn enhances the energy of

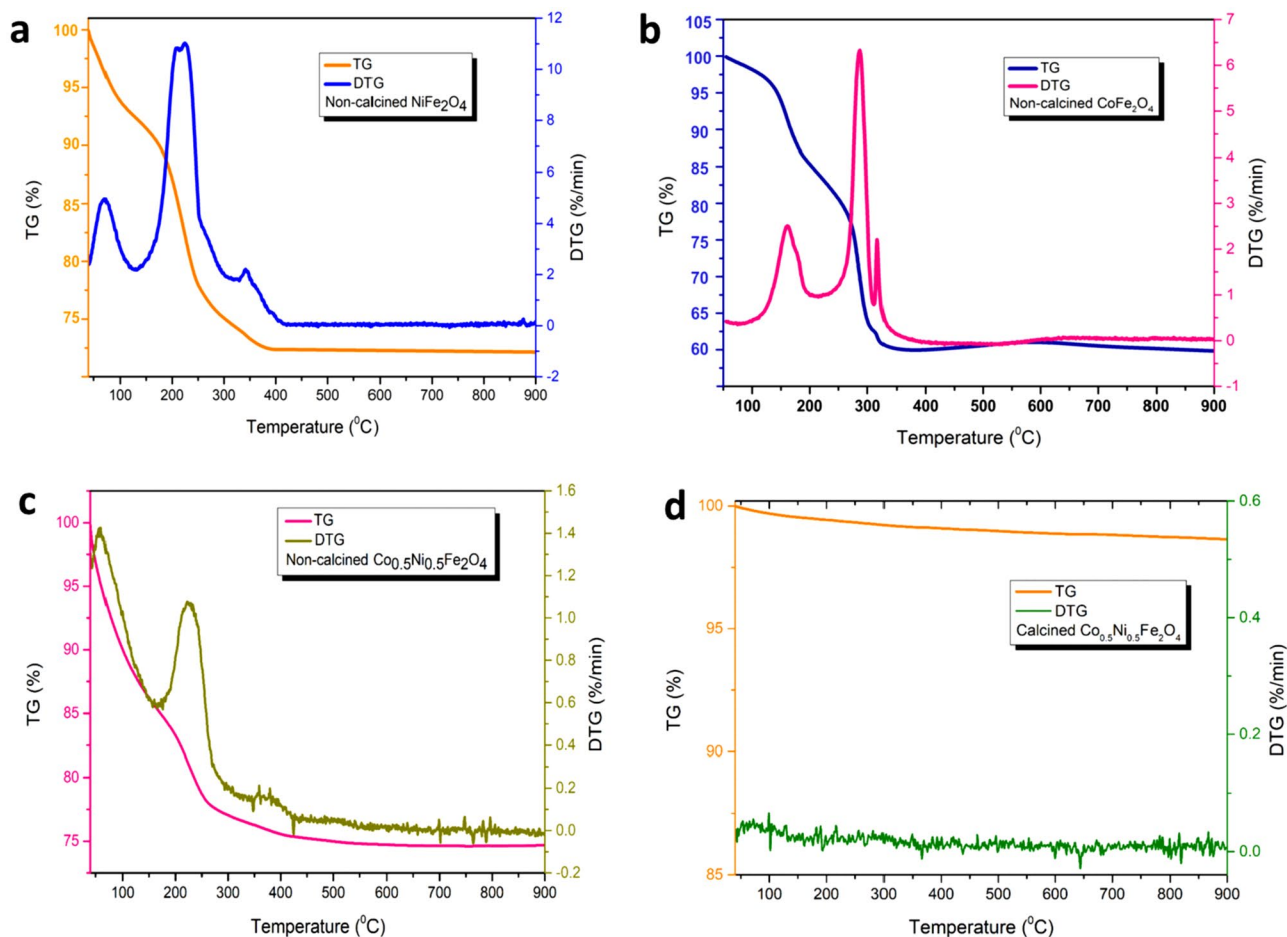


Fig. 8 TG/DTG curves of **a** non-calcined nickel ferrite (NiFe_2O_4), **b** non-calcined cobalt ferrite (CoFe_2O_4), **c** non-calcined cobalt nickel ferrite ($\text{Co}_{0.5}\text{Ni}_{0.5}\text{Fe}_2\text{O}_4$), and **d** calcined cobalt nickel ferrite ($\text{Co}_{0.5}\text{Ni}_{0.5}\text{Fe}_2\text{O}_4$)

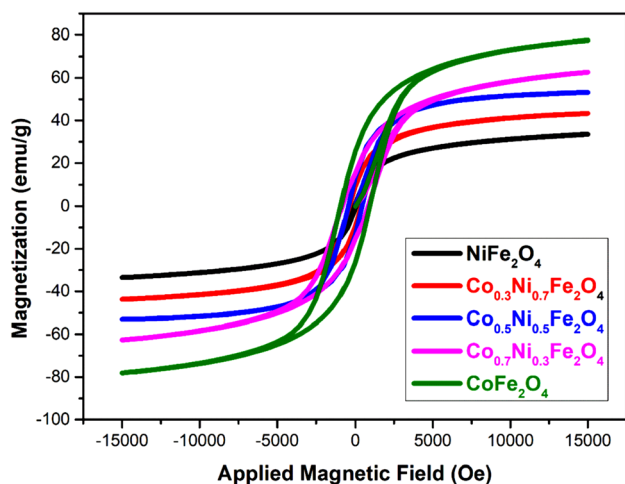


Fig. 9 Room temperature magnetization curves of $\text{Co}_x\text{Ni}_{1-x}\text{Fe}_2\text{O}_4$ ($x=0, 0.3, 0.5, 0.7, \text{ and } 1$)

Table 3 Magnetic parameters of $\text{Co}_x\text{Ni}_{1-x}\text{Fe}_2\text{O}_4$

Composition	H_c (Oe)	M_s (emu/g)	M_r (emu/g)	M_r/M_s
NiFe_2O_4	50.50	33.53	4.71	0.140
$\text{Co}_{0.3}\text{Ni}_{0.7}\text{Fe}_2\text{O}_4$	384.43	43.29	9.44	0.218
$\text{Co}_{0.5}\text{Ni}_{0.5}\text{Fe}_2\text{O}_4$	439.08	53.16	13.45	0.253
$\text{Co}_{0.7}\text{Ni}_{0.3}\text{Fe}_2\text{O}_4$	835.68	62.65	15.09	0.240
CoFe_2O_4	933.69	77.54	25.93	0.334

the domain wall. The improvement in the magnitudes of M_s and M_r can be interpreted based on Neel's theory and cations distribution at tetrahedral (A) and octahedral (B) sites. The electron spin of Fe ions at tetrahedral (A) and octahedral (B) sites are antiparallel to each other that cancel to form a net magnetic moment of $2 \mu_B$ due to Ni^{2+} ions at B sites. The dopant Co^{2+} ions with a magnetic moment of $3 \mu_B$ first occupy B sites. The enhancement in saturation magnetization (M_s) and remanent magnetization (M_r) emerges from the substitution of Ni ions (two unpaired electrons) with Co ions (three

unpaired electrons) that add the number of unpaired electrons at octahedral sites [37].

The magnitude of H_c ranges from 50.50 to 933.69 Oe with different cobalt concentrations shown in Table 3. The larger values of M_s and moderate H_c (as much as 600 Oe) are preferable for high-density recording media [50]. Our results have improved values for M_s and H_c . The samples having compositions Co_{0.3}Ni_{0.7}Fe₂O₄ and Co_{0.5}Ni_{0.5}Fe₂O₄ are promising materials for high-density recording media. Figure 10a depicts the variation of saturation magnetization (M_s) with an increase in cobalt contents. The graph shows a linear increment in M_s due to the high orbital contribution of cobalt ions in the magnetic moment. Cobalt ions are well known to yield high-induced anisotropy. Figure 10b and c depicts a variation of H_c and M_r , as a function of cobalt contents. The linear increase in coercivity (H_c) with cobalt content increment is because of the large coercivity affiliated with hard cobalt ferrite (CoFe₂O₄) structure and the anisotropic nature of cobalt ions. The enhancement in H_c may emerge from the exchanged anisotropy because of spin disorder at the particle surface, spin glass-like behavior in surface layers of nanoparticles due to chemical disorder, and the effect of spin canting. Coercivity originates from size, surface, shape, and magnetocrystalline anisotropy, hence depending upon synthetic conditions and size of the nanoparticles [59, 60].

Figure 10c indicates a weak increment in remanent magnetization (M_r) with an increase in cobalt contents correlated with small M_r affiliated with soft nickel ferrites. The improvement in remanence is preferably due to an increase in cobalt contents. Figure 10d represents the variation of M_s with particle sizes which reveals a linear increase in M_s . Figure 10e shows variation in M_r/M_s with cobalt composition known as squareness. The ratio of M_r/M_s increases with cobalt contents from 0.140 (NiFe₂O₄) to 0.334 (CoFe₂O₄). This suggests that the particles in all the samples interact via magnetostatic interactions ($R < 0.5$). In contrast, coherent rotations of randomly oriented, non-interacting particles occur for $R=0$ and the exchange-coupled exists when $R > 0.5$ [25]. The squareness is directly affected by magnetic anisotropy, crystal defect, particle size, and synthetic methods [37, 47]. The magnetization curve of samples synthesized without using malonic acid as a chelating agent is shown in Fig. S4 and parameters are tabulated in Table S2. The obtained results (XRD studies) show that without chelation the particle size (20.2–24.2 nm) is greater than with malonic acid chelation (7.9–15.4 nm). Magnetization for our samples is slightly higher than without chelation.

3.7 Impact of malonic acid as a chelating agent for the synthesis of cobalt–nickel ferrites

The malonic acid was used as a chelating agent for the preparation of cobalt ferrite, nickel ferrite, and cobalt–nickel

ferrites. It is observed from FTIR, XRD, and TG studies that malonic acid acts as a chelating agent for the synthesis of ferrites. Many chelating agents were used for the development of ferrites including citric acid, sago starch, EDTA, egg white, oxalic acid, tartaric acid, etc. [33, 34]. Some limitations were observed for chelating agents such as mixed phases of CoFe₂O₄ and α -Fe₂O₃ particles. The magnetization and coercivity were considerably decreased for the largest amount of sago because of the coexistence of the α -Fe₂O₃ phase with CoFe₂O₄ [33]. Polydispersed distribution with a wide range of particle size 80–200 nm was obtained with citric acid [32]. The magnetic properties of cobalt–nickel ferrite nanoparticles obtained using various chelating/capping agents are summarized in Table 4. Oleic acid shows high coercivity but M_s was reduced to 13.6 emu/g [61]. CoFe₂O₄ synthesized by using polyvinyl alcohol shows M_s values as 49.72 and 50 emu/g [62, 63], which in turn our sample gives a magnitude of M_s as 77.54 emu/gm. Nitrate ions/glycine (N/G) ratios were used for the synthesis of NiFe₂O₄, Ni_{0.5}Co_{0.5}Fe₂O₄, and CoFe₂O₄, the samples were calcined at 600 °C, and the M_s values obtained are 30.21, 43.50, and 52.63 emu/gm, respectively [64]; however, in case of our samples saturation magnetization significantly increased to 33.53, 53.16, and 77.54 emu/gm for the same composition of cobalt–nickel ferrites. This work suggests that these limitations such as mixed phases, polydispersed particles, and low M_s values can be overcome by using malonic acid as a chelating agent. It is observed from TEM studies that malonic acid gives a small range of particle size distribution (8–22 nm) for ferrite nanoparticles. A single ferrite phase is obtained from XRD analysis and no other oxide impurity is observed. This study suggests that malonic acid is a good chelating agent for small particle size distribution and single ferrite phase nanoparticles with high magnetic properties.

4 Conclusions

Cobalt–nickel ferrite nanoparticles (Co_xNi_{1-x}Fe₂O₄ where $x=0, 0.3, 0.5, 0.7, \text{ and } 1$) have been successfully synthesized via hydrothermal method using malonic acid as a chelating agent. The formation of spinel ferrite from the chelation complex (malonic acid: metal ions) has been confirmed by FTIR spectrum and thermal gravimetric studies. The two absorption bands obtained from the FTIR spectrum affirm the existence of A and B sublattices. Crystalline cubic spinel structure is confirmed by XRD analysis. The enhancement in the lattice parameter is attributed to larger ionic radii of Co²⁺ than Ni²⁺. The average crystallite size for cobalt–nickel ferrite nanoparticles calculated from XRD for CoFe₂O₄, Co_{0.5}Ni_{0.5}Fe₂O₄, and NiFe₂O₄ is 15.4, 10.1, and 7.9 nm, respectively. Monodispersed and non-uniform-shaped particles are observed for cobalt–nickel ferrites from

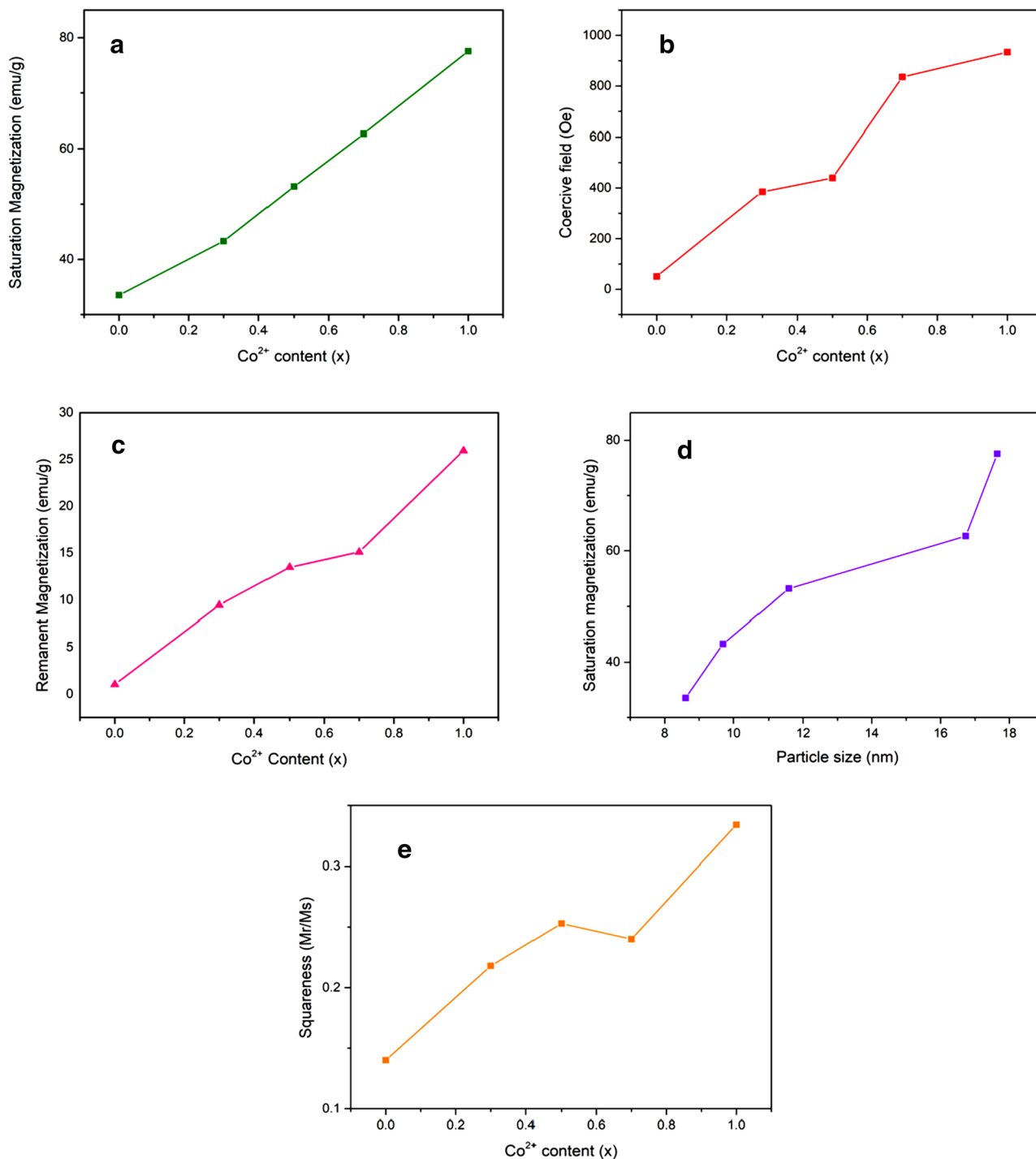


Fig. 10 **a** Variation of saturation magnetization with Co²⁺ content (Co_xNi_{1-x}Fe₂O₄), **b** variation of coercive field with Co²⁺ content (Co_xNi_{1-x}Fe₂O₄), **c** variation of remanent magnetization with Co²⁺

content (Co_xNi_{1-x}Fe₂O₄), **d** variation of saturation magnetization with particle size, and **e** variation of squareness parameter with Co²⁺ content (Co_xNi_{1-x}Fe₂O₄)

morphological studies. The presumed stoichiometry of samples matched very well with the calculated one interpreted from EDAX analysis. The XPS studies revealed oxidation states of cobalt, nickel, and iron as Co²⁺, Ni²⁺, and Fe³⁺. The effects of cobalt contents on magnetic properties have

been reported. The increase in saturation magnetization with cobalt contents is associated with the anisotropic nature of cobalt. The improved results for M_s and H_c for cobalt–nickel ferrite samples are useful for high-density recording media. A simple and easy hydrothermal method assisted with

Table 4 Saturation magnetization of ferrite nanoparticles by using different chelating/capping agents

Sr. No.	Chelating/capping agent	Ferrite composition	Annealing temperature °C	Saturation magnetization M_s (emu/g)	References
1.	Polyvinyl alcohol	CoFe ₂ O ₄	500	49.72	[62]
2.	Nitrate ions/glycine (N/G) ratios	NiFe ₂ O ₄	600	30.21	[64]
		Ni _{0.5} Co _{0.5} Fe ₂ O ₄		43.56	
		CoFe ₂ O ₄		52.63	
3.	Oleic acid	CoFe ₂ O ₄	500	13.6	[61]
4.	Sago starch (Metroxylonsagu)	CoFe ₂ O ₄	800	40–70	[33]
5.	Polyvinyl alcohol	CoFe ₂ O ₄	800	50	[63]
6.	EDTA	Ni _{0.2} Cu _{0.1} Co _{0.7} Fe ₂ O ₄	600	50.67	[34]
7.	Egg white			46.48	
8.	Oxalic acid			56.98	
9.	Tartaric acid			54.48	
10.	Citric acid			53.81	
11.	Polyvinyl pyrrolidone (PVP)	Co _{0.4} Ni _{0.6} Fe ₂ O ₄	600	43.35	[65]
12.	Malonic acid	NiFe ₂ O ₄	600	33.53	This work
		Co _{0.3} Ni _{0.7} Fe ₂ O ₄		43.29	
		Co _{0.5} Ni _{0.5} Fe ₂ O ₄		53.16	
		Co _{0.7} Ni _{0.3} Fe ₂ O ₄		62.65	
		CoFe ₂ O ₄		77.54	

malonic acid is convenient for the formation of cobalt–nickel ferrite nanostructure and samples achieved with improved magnetic properties are useful for potential applications.

Supplementary Information The online version contains supplementary material available at <https://doi.org/10.1007/s00339-022-06318-x>.

Acknowledgements We are thankful to UGC-DAE-CSR for providing financial support (CSR-IC-BL-67/CRS-184-2016-17/848 and CSR-IC-BL-38/CRS-135-2014-15/123). We are also thankful to Dr. Anil K. Sinha and Shri R. K. Sharma, Raja Raman Centre for Advanced Technology (RRCAT), Indore, for providing an instrumental facility. The authors are also thankful to DST for providing the DST-FIST Grant SR/FST/CSI-279/2016(C).

References

1. Y. Slimani, B. Unal, M.A. Almessiere, A.D. Korkmaz, S.E. Shirsath, G. Yasin, A.V. Trukhanov, A. Baykal, Investigation of structural and physical properties of Eu³⁺ ions substituted Ni_{0.4}Cu_{0.2}Zn_{0.4}Fe₂O₄ spinel ferrite nanoparticles prepared via sonochemical approach. *Results Phys.* **17**, 103061 (2020). <https://doi.org/10.1016/j.rinp.2020.103061>
2. M.A. Almessiere, Y. Slimani, H. Güngüne, S. Ali, A. Manikandan, I. Ercan, A. Baykal, A.V. Trukhanov, Magnetic attributes of NiFe₂O₄ nanoparticles: influence of dysprosium ions (Dy³⁺) substitution. *Nanomaterials* **9**, 820 (2019). <https://doi.org/10.3390/nano9060820>
3. M.A. Almessiere, Y. Slimani, M. Sertkol, M. Nawaz, A. Sadaqat, A. Baykal, I. Ercan, B. Özçelik, Effect of Nb³⁺ substitution on the structural, magnetic, and optical properties of Co_{0.5}Ni_{0.5}Fe₂O₄ nanoparticles. *Nanomaterials* **9**, 430 (2019). <https://doi.org/10.3390/nano9030430>
4. M.A. Almessiere, Y. Slimani, A.D. Korkmaz, A. Baykal, H. Güngüne, H. Sozeri, S.E. Shirsath, S. Guner, S. Akhtar, A. Manikandan, Impact of La³⁺ and Y³⁺ ion substitutions on structural, magnetic and microwave properties of Ni_{0.3}Cu_{0.3}Zn_{0.4}Fe₂O₄ nanospinel ferrites synthesized via sonochemical route. *RSC Adv.* **9**, 30671–30684 (2019). <https://doi.org/10.1039/C9RA06353F>
5. Q. Song, Z.J. Zhang, Shape control and associated magnetic properties of spinel cobalt ferrite nanocrystals. *J. Am. Chem. Soc.* **126**, 6164–6168 (2004). <https://doi.org/10.1021/ja049931r>
6. X. Bai, J. Wei, B. Tian, Y. Liu, T. Reiss, N. Guiblin, P. Gemeiner, B. Dkhil, I. C. Infante, Size effect on optical and photocatalytic properties in BiFeO₃ nanoparticles. *J. Phys. Chem. C* **120**, 3595–3601 (2016). <https://doi.org/10.1021/acs.jpcc.5b09945>
7. S.V. Bhandare, R. Kumar, A.V. Anupama, M. Mishra, R. V. Kumar, V.M. Jali, B. Sahoo, Effect of Mg-substitution in Co–Ni ferrites: cation distribution and magnetic properties. *Mater. Chem. Phys.* **251**, 123081 (2020). <https://doi.org/10.1016/j.matchemphys.2020.123081>
8. W. Hu, N. Qin, G. Wu, Y. Lin, S. Li, D. Bao, Opportunity of spinel ferrite materials in nonvolatile memory device applications based on their resistive switching performances. *J. Am. Chem. Soc.* **134**, 14658–14661 (2012). <https://doi.org/10.1021/ja305681n>
9. T.G. Glover, D. Sabo, L.A. Vaughan, J.A. Rossin, Z.J. Zhang, Adsorption of sulfur dioxide by CoFe₂O₄ spinel ferrite nanoparticles and corresponding changes in magnetism. *Langmuir* **28**, 5695–5702 (2012). <https://doi.org/10.1021/la3003417>
10. Y. Kumar, A. Sharma, P.M. Shirage, Shape-controlled CoFe₂O₄ nanoparticles as an excellent material for humidity sensing. *RSC Adv.* **7**, 55778–55785 (2017). <https://doi.org/10.1039/c7ra11072c>
11. V.K. Chakradhary, M.J. Akhtar, Absorption properties of CNF mixed cobalt nickel ferrite nanocomposite for radar and stealth applications. *J. Magn. Magn. Mater.* **525**, 167592 (2021). <https://doi.org/10.1016/j.jmmm.2020.167592>
12. F.M. Moghaddam, G. Tavakoli, A. Aliabadi, Application of nickel ferrite and cobalt ferrite magnetic nanoparticles in C–O bond formation: a comparative study between their catalytic

- activities. *RSC Adv.* **5**, 59142–59153 (2015). <https://doi.org/10.1039/C5RA08146G>
13. X. Lasheras, M. Insausti, I.G. Muro, E. Garaio, F. Plazaola, M. Moros, L.D. Matteis, J.M. Fuente, L. Lezama, Chemical synthesis and magnetic properties of monodisperse nickel ferrite nanoparticles for biomedical applications. *J. Phys. Chem. C* **120**, 3492–3500 (2016). <https://doi.org/10.1021/acs.jpcc.5b10216>
 14. M. Kaur, N. Kaur, Vibha, ferrites: synthesis and applications for environmental remediation. *ACS Symp. Ser.* **1238**, 113–136 (2016). <https://doi.org/10.1021/bk-2016-1238.ch004>
 15. T. F. Khan, U. Naresh, T. Ramprasad, R. J. Kumar, Structural, morphological, and magnetic properties of cobalt-doped nickel ferrite nanoparticles. *J. Supercond. Nov. Magn.* **34**, 797–803 (2021). <https://doi.org/10.1007/s10948-020-05788-5>
 16. A. Hajalilou, S.A. Mazlan, A review on preparation techniques for synthesis of nanocrystalline soft magnetic ferrites and investigation on the effects of microstructure features on magnetic properties. *Appl. Phys. A* **122**, 680 (2016). <https://doi.org/10.1007/s00339-016-0217-2>
 17. P. Coppola, F.G. da Silva, G. Gomide, F.L.O. Paula, A.F.C. Campos, R. Perzynski, C. Kern, J. Depuyrot, R. Aquino, Hydrothermal synthesis of mixed zinc–cobalt ferrite nanoparticles: structural and magnetic properties. *J. Nanopart. Res.* **18**, 138 (2016). <https://doi.org/10.1007/s11051-016-3430-1>
 18. G.S. Kumar, T. Raguram, K.S. Rajni, Synthesis and characterization of nickel-substituted cobalt ferrite nanoparticles using sol–gel auto-combustion method. *J. Supercond. Nov. Magn.* **32**, 1715–1723 (2019). <https://doi.org/10.1007/s10948-018-4867-5>
 19. S.S. Bharambe, A. Trimukhe, P. Bhatia, Synthesis techniques of nickel substituted cobalt ferrites—an investigative study using structural data. *Mater. Today: Proc.* **23**, 373–381 (2020). <https://doi.org/10.1016/j.matpr.2020.02.056>
 20. Z. Zhang, Y. Liu, G. Yao, G. Zu, Y. Hao, Synthesis and characterization of NiFe₂O₄ nanoparticles via solid-state reaction. *Int. J. Appl. Ceram. Technol.* **10**, 142–149 (2013). <https://doi.org/10.1111/j.1744-7402.2011.02719.x>
 21. M. Houshiar, F. Zebhi, Z.J. Razi, A. Alidoust, Z. Askari, Synthesis of cobalt ferrite (CoFe₂O₄) nanoparticles using combustion, coprecipitation, and precipitation methods: a comparison study of size, structural, and magnetic properties. *J. Magn. Mater.* **371**, 43–48 (2014). <https://doi.org/10.1016/j.jmmm.2014.06.059>
 22. C.R. Vestal, Z.J. Zhang, Synthesis of CoCrFeO₄ nanoparticles using microemulsion methods and size-dependent studies of their magnetic properties. *Chem. Mater.* **14**, 3817–3822 (2002). <https://doi.org/10.1021/cm020112k>
 23. M. Sedlar, L. Pust, Preparation of cobalt doped nickel ferrite thin films on optical fibers by dip-coating technique. *Ceram. Int.* **21**, 21–27 (1995). [https://doi.org/10.1016/0272-8842\(95\)93267-7](https://doi.org/10.1016/0272-8842(95)93267-7)
 24. P.P. Hankare, K.R. Sanadi, K.M. Garadkar, D.R. Patil, I.S. Mulla, Synthesis and characterization of nickel substituted cobalt ferrite nanoparticles by sol–gel auto-combustion method. *J. Alloys Compd.* **553**, 383–388 (2013). <https://doi.org/10.1016/j.jallcom.2012.11.181>
 25. K. Maaz, A. Mumtaz, S.K. Hasanain, A. Ceylan, Synthesis and magnetic properties of cobalt ferrite (CoFe₂O₄) nanoparticles prepared by wet chemical route. *J. Magn. Mater.* **308**, 289–295 (2007). <https://doi.org/10.1016/j.jmmm.2006.06.003>
 26. J. Huo, M. Wei, Characterization and magnetic properties of nanocrystalline nickel ferrite synthesized by hydrothermal method. *Mater. Lett.* **63**, 1183–1184 (2009). <https://doi.org/10.1016/j.matlet.2009.02.024>
 27. S. Jovanović, M. Spreitzer, M. Otoničar, J. Jeon, D. Suvorov, pH control of magnetic properties in precipitation-hydrothermal-derived CoFe₂O₄. *J. Alloys Compd.* **589**, 271–277 (2014). <https://doi.org/10.1016/j.jallcom.2013.11.217>
 28. M. Srivastava, S. Chaubey, A.K. Ojha, Investigation on size dependent structural and magnetic behavior of nickel ferrite nanoparticles prepared by sol–gel and hydrothermal methods. *Mater. Chem. Phys.* **118**, 174–180 (2009). <https://doi.org/10.1016/j.matchemphys.2009.07.023>
 29. A. Hajalilou, S. A. Mazlan, M. Abbasi, H. Lavvafi, Fabrication of spherical CoFe₂O₄ nanoparticles via sol–gel and hydrothermal methods and investigation of their magnetorheological characteristics. *RSC Adv.* **6**, 89510–89522 (2016). <https://doi.org/10.1039/C6RA13493A>
 30. M. Yoshimura, K. Byrappa, Hydrothermal processing of materials: past, present and future. *J. Mater. Sci.* **43**, 2085–2103 (2008). <https://doi.org/10.1007/s10853-007-1853-x>
 31. M.M.L. Sonia, S. Anand, S. Blessi, S. Pauline, A. Manikandan, Effect of surfactants (PVB/EDTA/CTAB) assisted sol–gel synthesis on structural, magnetic and dielectric properties of NiFe₂O₄ nanoparticles. *Ceram. Int.* **44**, 22068–22079 (2018). <https://doi.org/10.1016/j.ceramint.2018.08.317>
 32. M. Sajjia, M. Oubaha, T. Prescott, A.G. Olabi, Development of cobalt ferrite powder preparation employing the sol–gel technique and its structural characterization. *J. Alloys Compd.* **506**, 400–406 (2010). <https://doi.org/10.1016/j.jallcom.2010.07.015>
 33. A. Hunyek, C. Sirisathitkul, C. Mahaphap, U. Boonyang, W. Tangwatanakul, Sago starch: chelating agent in sol–gel synthesis of cobalt ferrite nanoparticles. *J. Aust. Ceram. Soc.* **53**, 173–176 (2017). <https://doi.org/10.1007/s41779-017-0022-1>
 34. W. Zhang, A. Sun, X. Zhao, X. Pan, Y. Han, N. Suo, L. Yu, Z. Zuo, Structural and magnetic properties of Ni–Cu–Co ferrites prepared from sol–gel auto combustion method with different complexing agents. *J. Alloys Compd.* **816**, 152501 (2020). <https://doi.org/10.1016/j.jallcom.2019.152501>
 35. A.S. Nikolic, N. Jovic, J. Rogan, A. Kremenovic, M. Ristic, A. Meden, B. Antic, Carboxylic acids and polyethylene glycol assisted synthesis of nanocrystalline nickel ferrites. *Ceram. Int.* **39**, 6681–6688 (2013). <https://doi.org/10.1016/j.ceramint.2013.01.106>
 36. A. Soldner, J. Zach, M. Iwanow, T. Gartner, M. Schlosser, A. Pfitzner, B. Konig, Preparation of magnesium, cobalt and nickel ferrite nanoparticles from metal oxides using deep eutectic solvents. *Chem. Eur. J.* **22**, 13108–13113 (2016). <https://doi.org/10.1002/chem.201602821>
 37. A. Ati, Z. Othaman, A. Samavati, Influence of cobalt on structural and magnetic properties of nickel ferrite nanoparticles. *J. Mol. Struct.* **1052**, 177–182 (2013). <https://doi.org/10.1016/j.molstruc.2013.08.040>
 38. M. Sivakumar, S. Kanagesan, K. Chinnaraj, R.S. Babu, S. Nithyanantham, Synthesis, characterization and effects of citric acid and PVA on magnetic properties of CoFe₂O₄. *J. Inorg. Organomet. Polym.* **23**, 439–445 (2013). <https://doi.org/10.1007/s10904-012-9801-x>
 39. A. Sutka, R. Pärna, G. Mezinskis, V. Kisand, Effects of Co ion addition and annealing conditions on nickel ferrite gas response. *Sens. Actuators B Chem.* **192**, 173–180 (2014). <https://doi.org/10.1016/j.snb.2013.10.077>
 40. A.A. Ati, Fast synthesis, structural, morphology with enhanced magnetic properties of cobalt doped nickel ferrite nanoscale. *J. Mater. Sci. Mater. Electron.* **29**, 12010–12021 (2018). <https://doi.org/10.1007/s10854-018-9305-8>
 41. S.T. Assar, H.F. Abosheisha, Structure and magnetic properties of Co–Ni–Li ferrites synthesized by citrate precursor method. *J. Magn. Mater.* **324**, 3846–3852 (2012). <https://doi.org/10.1016/j.jmmm.2012.06.033>
 42. L. Gao, E. Han, Y. He, C. Du, J. Liu, X. Yang, Effect of different templating agents on cobalt ferrite (CoFe₂O₄) nanomaterials for high-performance supercapacitor. *Ionics* **26**, 3643–3654 (2020). <https://doi.org/10.1007/s11581-020-03482-z>

43. T.M.L. Alves, B.F. Amorim, M.A.M. Torres, C.G. Bezerra, S.N. Medeiros, P.L. Gastelois, L.E.F. Outon, W.A.A. Macedo, Wasp-waisted behavior in magnetic hysteresis curves of CoFe₂O₄ nanopowder at a low temperature: experimental evidence and theoretical approach. *RSC Adv.* **7**, 22187–22196 (2017). <https://doi.org/10.1039/c6ra28727a>
44. N.S. McIntyre, D.G. Zetaruk, X-ray photoelectron spectroscopic studies of iron oxides. *Anal. Chem.* **49**, 1521–1529 (1977). <https://doi.org/10.1021/ac50019a016>
45. B.J. Tan, K.J. Klabunde, P.M.A. Sherwood, XPS studies of solvated metal atom dispersed (SMAD) catalysts. Evidence for layered cobalt–manganese particles on alumina and silica. *J. Am. Chem. Soc.* **113**, 855–861 (1991). <https://doi.org/10.1021/ja0003a019>
46. R. Pärna, U. Joost, E. Nõmmiste, T. Käämbre, A. Kikas, I. Kuusik, M. Hirsimäki, I. Kink, V. Kisand, Effect of cobalt doping and annealing on properties of titania thin films prepared by sol–gel process. *Appl. Surf. Sci.* **257**, 6897–6907 (2011). <https://doi.org/10.1016/j.apsusc.2011.03.026>
47. M. Gharagozlou, Synthesis, characterization and influence of calcination temperature on magnetic properties of nanocrystalline spinel Co-ferrite prepared by polymeric precursor method. *J. Alloys Compd.* **486**, 660–665 (2009). <https://doi.org/10.1016/j.jallcom.2009.07.025>
48. F.J. Caires, L.S. Lima, C.T. Carvalho, R.J. Giagio, M. Ionashiro, Thermal behaviour of malonic acid, sodium malonate and its compounds with some bivalent transition metal ions. *Thermochim. Acta* **497**, 35–40 (2010). <https://doi.org/10.1016/j.tca.2009.08.013>
49. J. Smit, H.P.J. Wijn, *Ferrites: physical properties of ferrimagnetic oxides in relation to their technical applications* (Cleaver-Hume Press, London, 1959)
50. R. Muller, W. Schuppel, Co spinel ferrite powders prepared by glass crystallization. *J. Magn. Magn. Mater.* **155**, 110–112 (1996). [https://doi.org/10.1016/0304-8853\(95\)00672-9](https://doi.org/10.1016/0304-8853(95)00672-9)
51. E. Manova, T. Tsoncheva, C.I. Estournès, D. Paneva, K. Tenchev, I. Mitov, L. Petrov, Nanosized iron and iron–cobalt spinel oxides as catalysts for methanol decomposition. *Appl. Catal. A Gen.* **300**, 170–180 (2006). <https://doi.org/10.1016/j.apcata.2005.11.005>
52. G. Li, Y. Jiang, K. Huang, P. Ding, J. Chen, Preparation and properties of magnetic Fe₃O₄–chitosan nanoparticles. *J. Alloys Compd.* **466**, 451–456 (2008). <https://doi.org/10.1016/j.jallcom.2007.11.100>
53. V. Marghussian, 4. Magnetic properties of nano-glass ceramics, in *Nano-glass ceramics*. ed. by V. Marghussian (Elsevier, Amsterdam, 2015), pp.181–223. <https://doi.org/10.1016/B978-0-323-35386-1.00004-9>
54. K. Nejati, R. Zabihi, Preparation and magnetic properties of nano size nickel ferrite particles using hydrothermal method. *Chem. Cent. J.* **6**, 23 (2012). <https://doi.org/10.1186/1752-153X-6-23>
55. Y.W. Ju, J.H. Park, H.R. Jung, S.J. Cho, W.J. Lee, Fabrication and characterization of cobalt ferrite (CoFe₂O₄) nanofibers by electrospinning. *Mater. Sci. Eng. B* **147**, 7–12 (2008). <https://doi.org/10.1016/j.mseb.2007.10.018>
56. R.C. Kambale, P.A. Shaikh, S.S. Kamble, Y.D. Kolekar, Effect of cobalt substitution on structural, magnetic and electric properties of nickel ferrite. *J. Alloys Compd.* **478**, 599–603 (2009). <https://doi.org/10.1016/j.jallcom.2008.11.101>
57. V. Pillai, D.O. Shah, Synthesis of high-coercivity cobalt ferrite particles using water-in-oil microemulsions. *J. Magn. Magn. Mater.* **163**, 243–248 (1996). [https://doi.org/10.1016/S0304-8853\(96\)00280-6](https://doi.org/10.1016/S0304-8853(96)00280-6)
58. A. Pradeep, P. Priyadharsini, G. Chandrasekaran, Production of single phase nano size NiFe₂O₄ particles using sol–gel auto combustion route by optimizing the preparation conditions. *Mater. Chem. Phys.* **112**, 572–576 (2008). <https://doi.org/10.1016/j.matchemphys.2008.05.090>
59. Y. Köseoglu, M. Bay, M. Tan, A. Baykal, H. Sözeri, R. Topkaya, N. Akdoğan, Magnetic and dielectric properties of Mn_{0.2}Ni_{0.8}Fe₂O₄ nanoparticles synthesized by PEG-assisted hydrothermal method. *J. Nanopart. Res.* **13**, 2235–2244 (2011)
60. S. Joshi, M. Kumar, Effect of Ni²⁺ substitution on structural, magnetic, dielectric and optical properties of mixed spinel CoFe₂O₄ nanoparticles. *Ceram. Int.* **42**, 18154–18165 (2016). <https://doi.org/10.1016/j.ceramint.2016.08.130>
61. M.V. Limaye, S.B. Singh, S.K. Date, D. Kothari, V.R. Reddy, A. Gupta, V. Sathe, R.J. Choudhary, S.K. Kulkarni, High coercivity of oleic acid capped CoFe₂O₄ nanoparticles at room temperature. *J. Phys. Chem. B* **113**, 9070–9076 (2009). <https://doi.org/10.1021/jp810975v>
62. K.S. Rao, G.S.V.R.K. Choudary, K.H. Rao, C. Sujatha, Structural and magnetic properties of ultrafine CoFe₂O₄ nanoparticles. *Procedia Mater. Sci.* **10**, 19–27 (2015). <https://doi.org/10.1016/j.mspro.2015.06.019>
63. A. Hunyok, C. Sirisathitkul, P. Harding, D.J. Harding, Structural and magnetic properties of cobalt ferrites synthesized using sol–gel techniques. *Mater. Sci.* **30**, 278–281 (2012). <https://doi.org/10.2478/s13536-012-0035-y>
64. J.L.O. Quiñonez, U. Pal, M.S. Villanueva, Structural, magnetic, and catalytic evaluation of spinel Co, Ni, and Co–Ni ferrite nanoparticles fabricated by low-temperature solution combustion process. *ACS Omega* **3**, 14986–15001 (2018). <https://doi.org/10.1021/acsomega.8b02229>
65. V.K. Chakradhary, A. Ansari, M.J. Akhtar, Design, synthesis, and testing of high coercivity cobalt doped nickel ferrite nanoparticles for magnetic applications. *J. Magn. Magn. Mater.* **469**, 674–680 (2019). <https://doi.org/10.1016/j.jmmm.2018.09.021>

Publisher's Note Springer Nature remains neutral with regard to jurisdictional claims in published maps and institutional affiliations.

Springer Nature or its licensor (e.g. a society or other partner) holds exclusive rights to this article under a publishing agreement with the author(s) or other rightsholder(s); author self-archiving of the accepted manuscript version of this article is solely governed by the terms of such publishing agreement and applicable law.